Supporting Information for "The Green's Function Model Intercomparison Project (GFMIP) Protocol"

Jonah Bloch-Johnson[1], Maria A. A. Rugenstein[2], Marc J. Alessi[2], Cristian Proistosescu[3], Ming Zhao[4], Bosong Zhang[5], Andrew I. L. Williams[6], Jonathan M. Gregory[1,7], Jason Cole[8], Yue Dong[9], Margaret L. Duffy[10], Sarah M. Kang[11], and Chen Zhou[12]

[1]National Center for Atmosphere Science, University of Reading, Reading, UK

[2]Department of Atmospheric Science, Colorado State University, Fort Collins, CO, USA

[3]Department of Atmospheric Sciences and Department of Earth Sciences and Environmental Change, University of Illinois, Urbana-Champaign, Urbana, IL, USA

[4]NOAA Geophysical Fluid Dynamics Laboratory, Princeton, NJ, USA

[5]Program in Atmospheric and Oceanic Sciences, Princeton University, Princeton, NJ, USA

[6]Atmospheric, Oceanic and Planetary Physics, Department of Physics, University of Oxford, Oxford, UK

[7]Met Office Hadley Centre, Exeter, UK

[8]Canadian Centre for Climate Modelling and Analysis, Environment and Climate Change Canada, Victoria, BC, Canada

[9]Lamont-Doherty Earth Observatory, Columbia University, Palisades, NY, USA

[10]National Center for Atmospheric Research, Boulder, CO, USA

[11]Department of Urban and Environmental Engineering, Ulsan National Institute of Science and Technology, Ulsan, South Korea

[12]Department of Atmospheric Physics, Nanjing University, Nanjing, China

This document contains ten figures and one table:

• Figure S1 shows derivatives of $\overline{N}$ over the tropical Pacific case study region using the CanESM5, HadAM3, and ICON models.

• Figure S2 shows the results of using monthly and seasonal averages as opposed to annual averages when performing the Green's function method.

• Figure S3 shows the results of using different CO_2 concentrations as the background concentration.

• Figure S4 shows the time series of $\overline{N}$ in the control simulation performed using the HadCM3 piControl base state.

• Figure S5 rescales points in the paper's Figure 5 to test relationships from the analytic formula for uncertainty (Equation 7 in the main body of the paper).

• Figure S6 shows reconstructions of the response of $\overline{N}$ to historical and abrupt4x patterns of $\overrightarrow{SST}$ change with only warming or cooling patches, i.e. $A_p \in \{+4, +2, -2, -4\}$K.

• Figure S7 shows derivatives calculated for a case study to determine if equal-area patches can be used around the Southern Ocean instead of equal-lat./lon. patches.

• Figure S8 shows results analogous to Figure 6 in the main body of the paper, except using rectangular patches instead of sinusoidal ones.

• Figure S9 shows the results of using the derivatives from Figure S1 to reconstruct the response of $\overline{N}$ to the historical and abrupt4x patterns of $\overrightarrow{SST}$ change.

• Figure S10 tests whether HadAM3's response of $\overline{N}$ to the full pattern of historical and abrupt4x temperature changes is the sum of its responses to these patterns' decompositions into uniform perturbation and zero-mean patterns.

• Table S1 documents the patch layouts used in the tropical case study (i.e., Figure 6 in the main body of the paper and Figure S8 below).

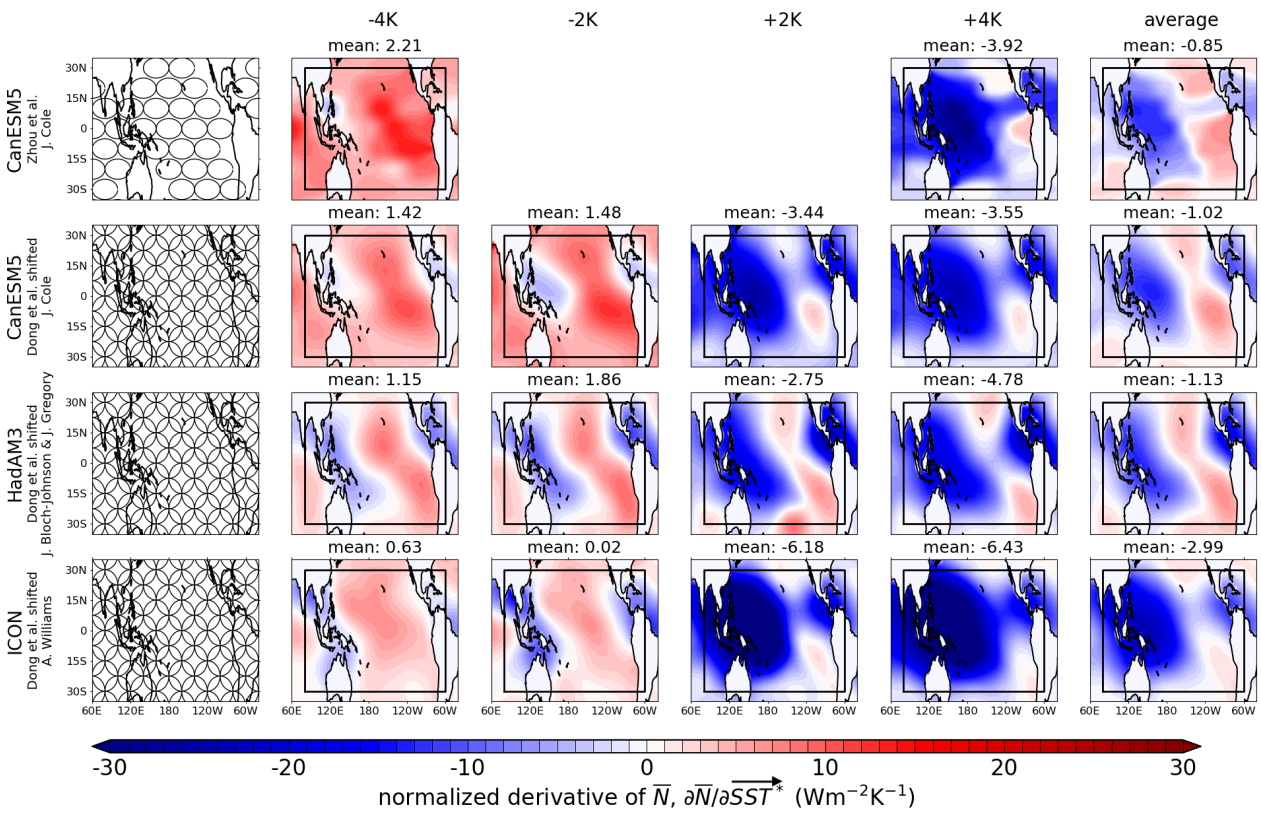

Figure S1. Derivatives of $\overline{N}$ over the tropical Pacific (100°W to 60°E and 30°S to 30°N) for CanESM5 and ICON run using the "Dong et al. shifted" patch layout, along with the CanESM5 "Zhou et al." layout from Figure 2 and the HadAM3 "Dong et al. shifted" layout from Figure 5 in the main body of the paper. The map in the last column shows the average of the rest of the derivatives in a given row. The first two rows illustrates how differences in patch layout can affect derivatives, while the last three rows show how differences in model physics can affect derivatives. Note that ICON has qualitatively similar features over the tropical Pacific to the models in Figure 2.

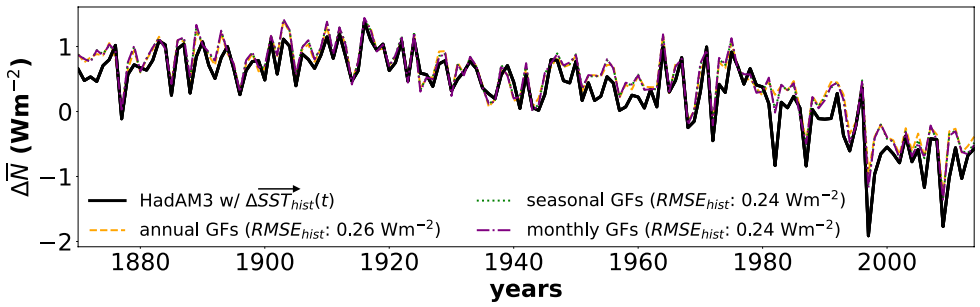

Figure S2. Green's function reconstructions of the response of HadAM3's $\overline{N}$ to historical $\overrightarrow{SST}$ changes. The reconstructions use the GFMIP protocol but differ in that for the dashed orange lines, a single, annually averaged derivative is used, while for the purple dot-dash lines, a seperate derivative is estimated for each month of the year and applied in rotation to a monthly $\overrightarrow{SST}$ time series before an annual average is taken. For the green dotted lines, the same calculation is made, but for seasonal values. There is little difference in $RMSE_{hist}$, and so for simplicity in this study we use annually averaged derivatives.

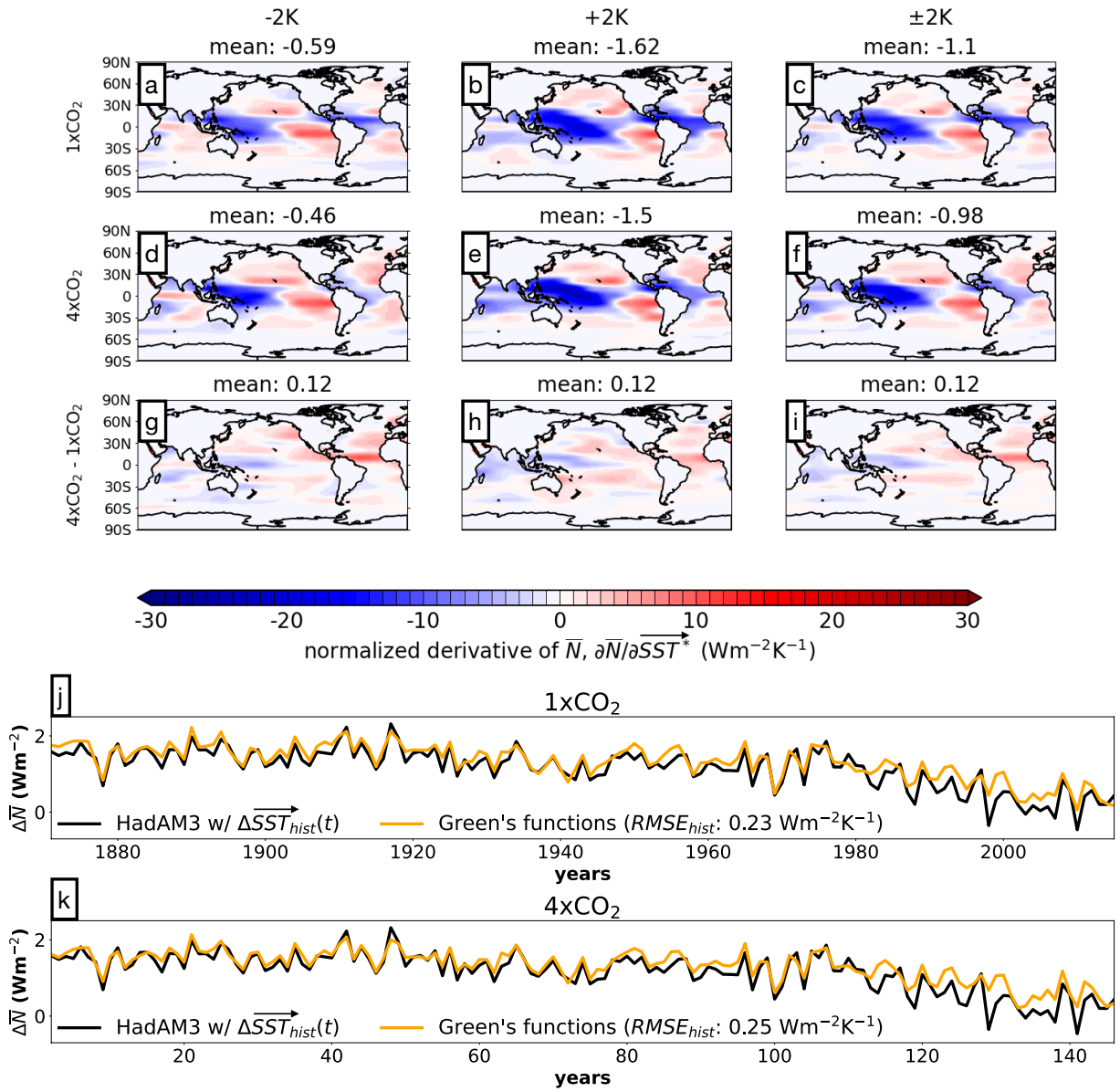

Figure S3. Panels a-f show derivatives of $\overline{N}$ estimated for HadAM3, with a range of values of A_p, and with CO_2 concentrations of 280ppm (panels a-c) and 1120ppm (panels d-f). Derivatives were calculated with respect to the AMIP base state, such that panel c in this figure is identical to panel g in Figure 4 in the main body of the paper. Panels g-i show the effect of increasing the CO_2 concentration on the derivative of $\overline{N}$. Panel j in this figure is identical to panel h in Figure 4 in the main body of the paper, while panel k shows the same except using the derivatives from panel f in the Green's function estimate.

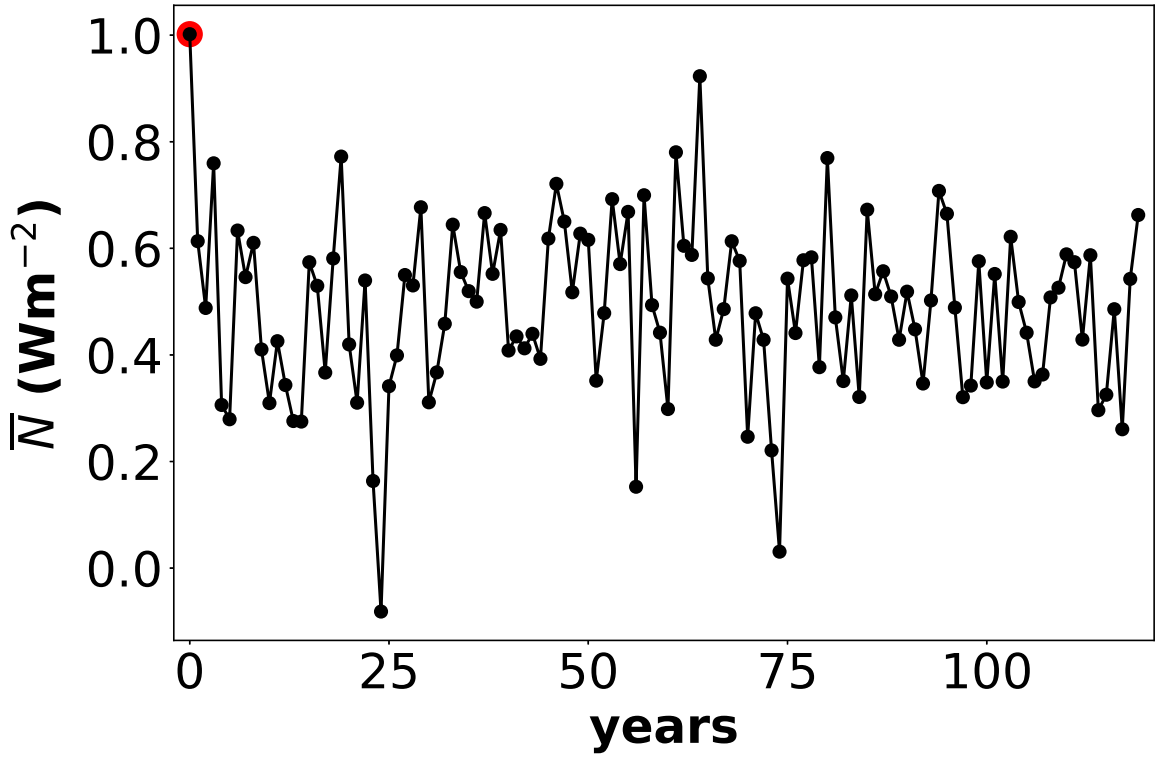

Figure S4. A time series of the HadAM3 control simulation performed with the "HadCM3 piControl" base state climatology. Note that the initial year is an outlier (red dot), suggesting that the model may be out of equilibrium during this year due to initial conditions.

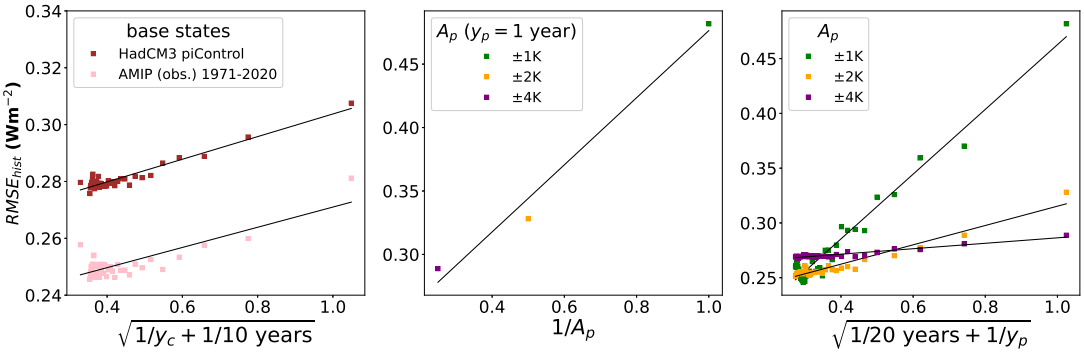

Figure S5. Values from Figure 5 in the main body of the paper rescaled according to the paper's Equation 7, showing that the error roughly scales with the square root of the sum of the inverses of the number of control simulation years, y_c, and patch simulation years, y_p (left panel varies y_c, right panel varies y_p). The middle panel shows the variation of error with $1/A_p$ when $y_p = 1$ year (for higher values of y_p, the nonlinearity associated with $A_p = \pm 4$K causes its error to surpass the other values).

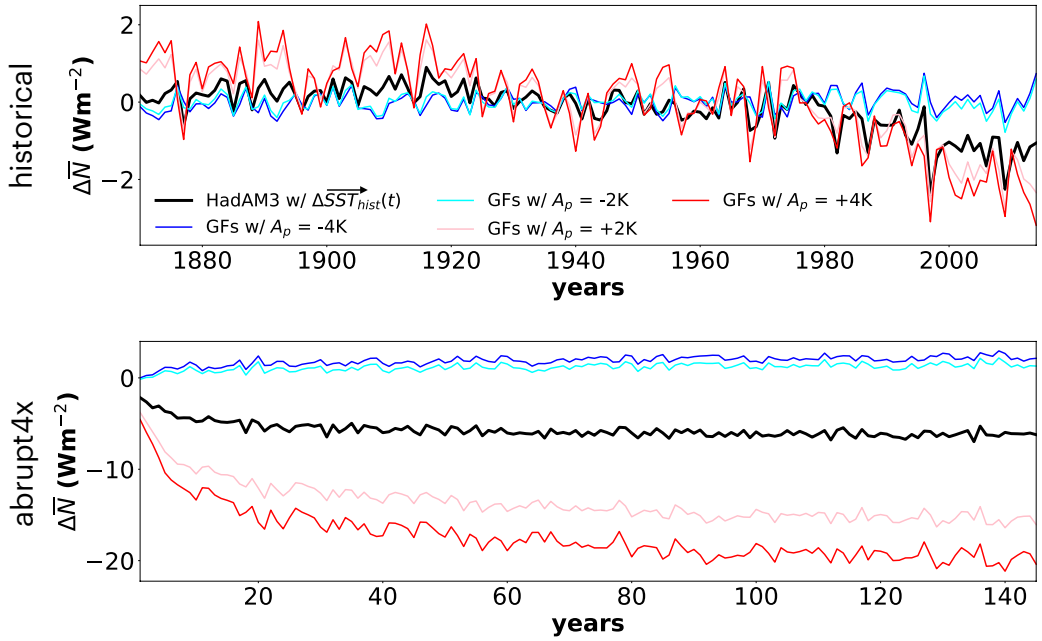

Figure S6. HadAM3's ensemble-mean response of $\overline{N}$ (black lines) to historical (top row) and abrupt4x patterns of warming, as well as their reconstructions using the Green's function method with the GFMIP protocol, except only warming or cooling patches are used; i.e. $A_p \in \{+4, +2, -2, -4\}$K (colored lines). Derivatives using patches of a single sign result in much poorer reconstructions of $\Delta\overline{N}$ than those using averages (e.g., see Figure 8 in the main body of the paper).

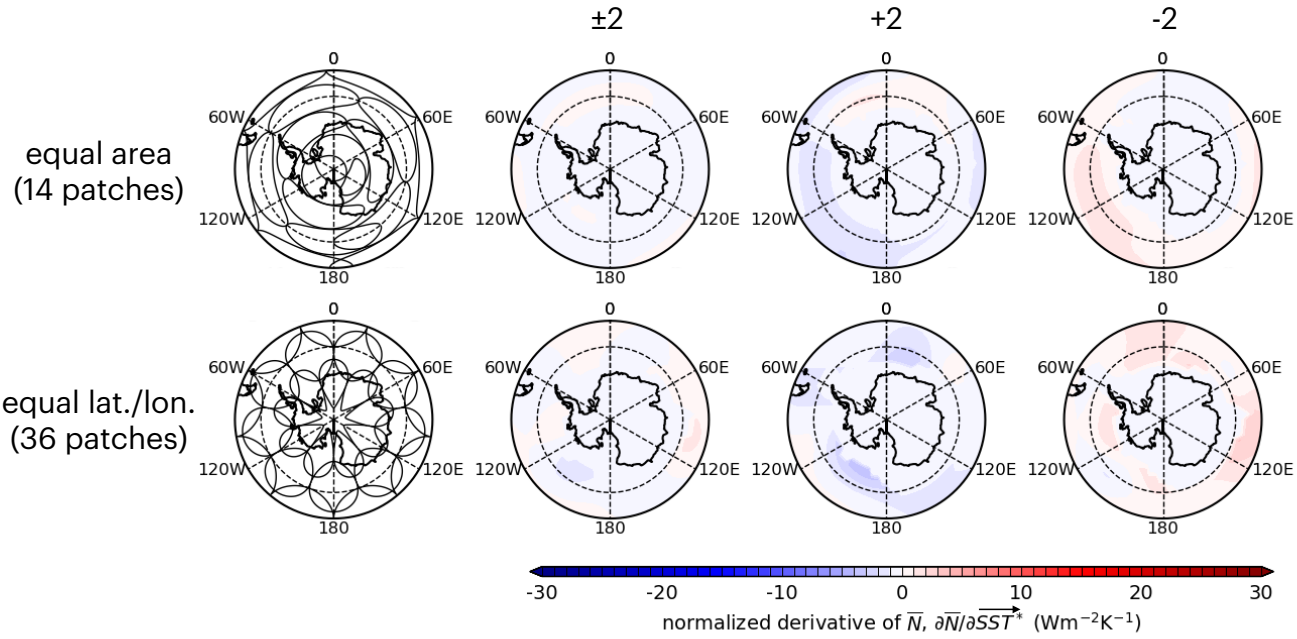

Figure S7. Normalized derivatives of $\overline{N}$ with respect to sea surface temperatures around the Southern Ocean made using an equal area (top row) and an equal latitude/longitude (bottom row) patch layout. The left column shows the half-amplitude of the different patches as in the top row of Figure 2, while the next three columns show the derivatives associated with $A_p = +2$K (third column), -2K (fourth column), and their average (second column). The scale of the colorbar is chosen to be consistent with the other figures in the main body of the paper.

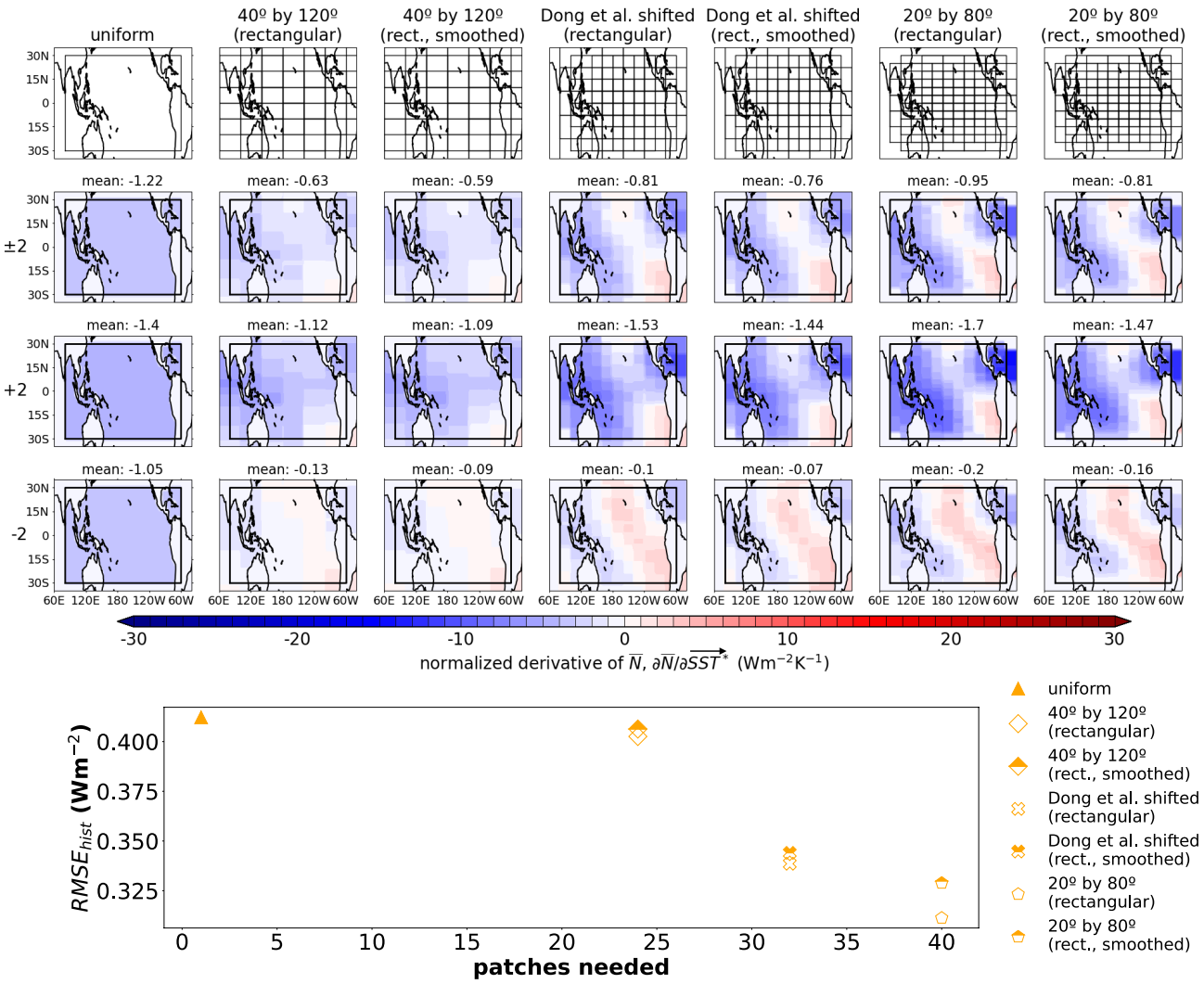

Figure S8. The same as Figure 6 in the main body of the paper, but with rectangular patches, where "(rectangular)" in a layout name indicates patches consist of a uniform perturbation of A_p over the whole patch area with a step function at the edge, and "(rect., smoothed)" is the same but with a tanh function with e-folding scale of 1° at the patch edges. Note that sinusoidal patches have much more strongly peaked warming in their centers, so that rectangular patches behave similarly to sinusoidal patches with a larger size (e.g., they have less asymmetry with respect to cooling vs. warming derivatives than patches with the same $\delta\phi_p$ and $\delta\theta_p$).

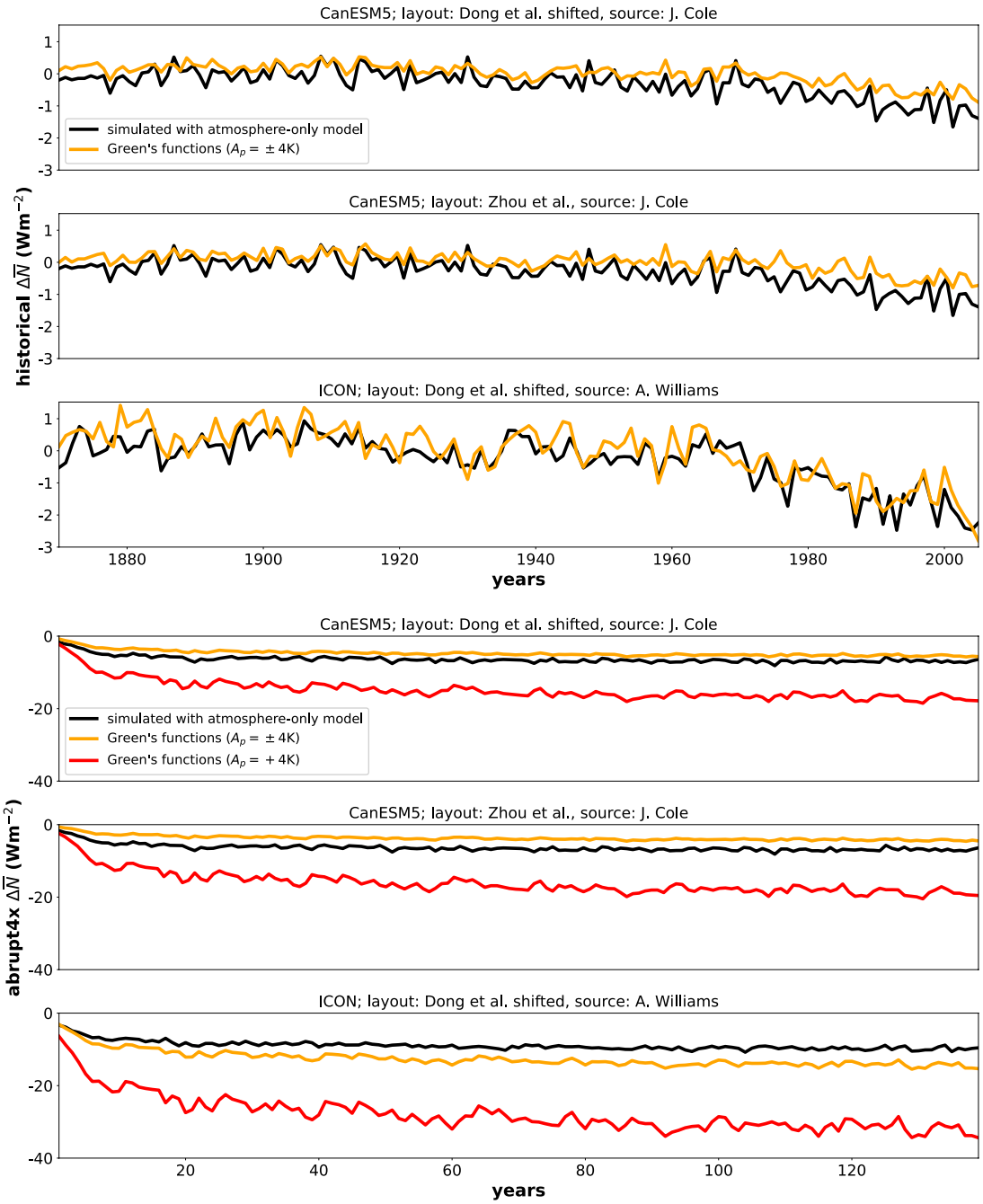

Figure S9. Like the full-pattern time series in Figure 8, except that the *SST* perturbations only occur over the tropical Pacific case study region (100°W to 60°E and 30°S to 30°N), and the Green's function estimates are made using the non-HadAM3 derivatives in Figure S1. Note that all of the Green's functions estimates made using just warming patches (red lines) overestimate the magnitude of the response to the abrupt4x pattern of warming.

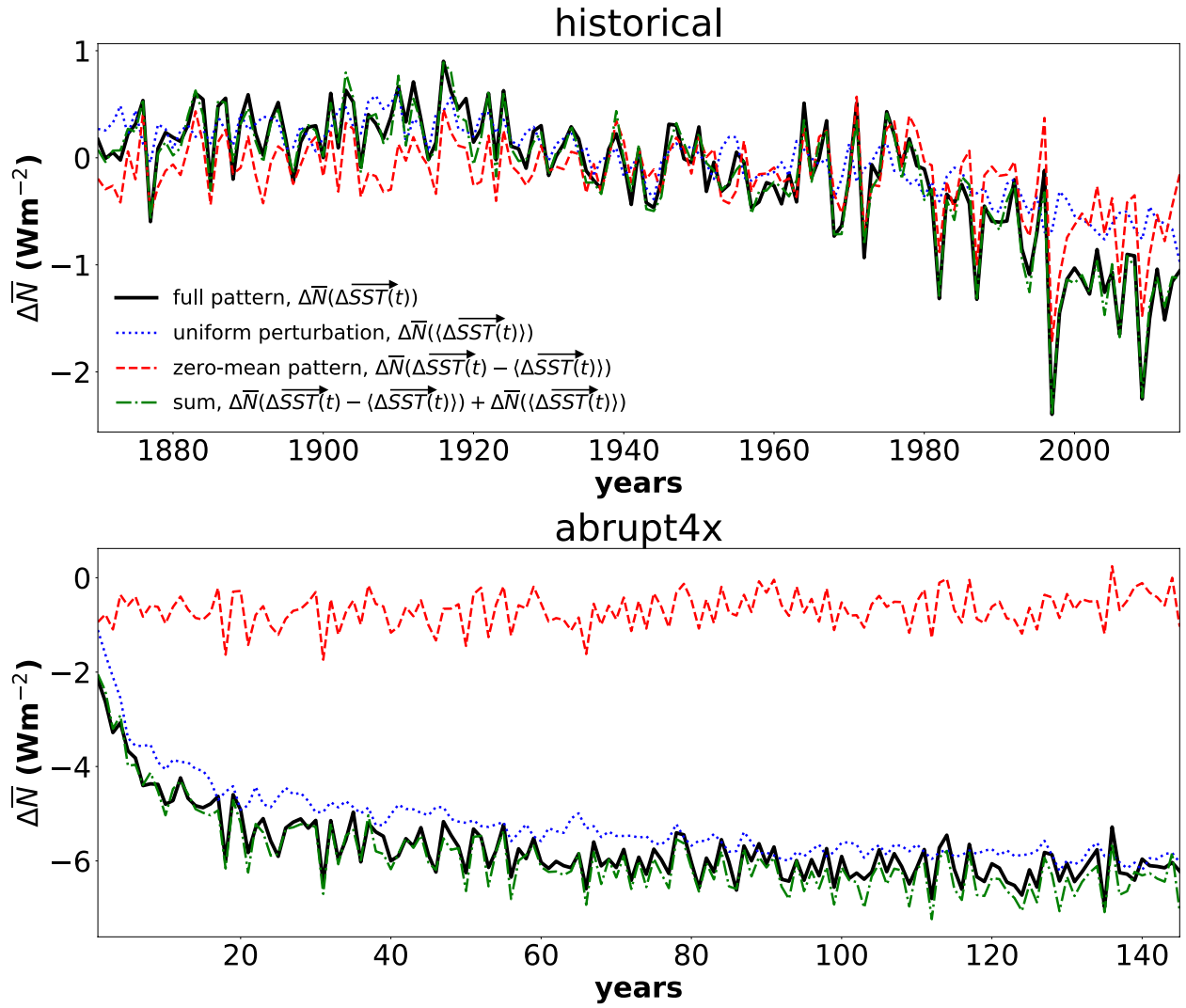

Figure S10. A test of the linearity of decomposing the response of $\overline{N}$ in HadAM3 to patterns of $\overrightarrow{SST}$ change into responses to uniform and zero-mean components. Black solid lines show the response of $\overline{N}$ to the full pattern of warming; blue dotted lines show the responses of $\overline{N}$ to a uniform perturbation with the same ice-free-ocean mean value as the full pattern; red dashed lines show the response to the zero-mean pattern, which is the anomaly of the full pattern with respect to its ocean mean; and the green lines with alternating dots and dashes show the sums of the blue dotted lines and red dashed lines. Linearity holds fairly well (that is, the black and green lines are similar), even for the the abrupt4x pattern.

Table S1. Tropical Pacific patch setups (covering 100°W to 60°E, 30°S to 30°N) as shown in Figure 6 in the main body of the paper and Figure S8 above.

Name	Size	Locations
60° by 160°	$\delta\phi_p = 60°$	$\lvert\phi_p\rvert \in \{0°, 30°\},\ \theta_p \in \{80°\text{E, then every } 80° \text{ eastwards}\}$
	$\delta\theta_p = 160°$	$\lvert\phi_p\rvert = 15°,\ \theta_p \in \{120°\text{E, then every } 80° \text{ eastwards}\}$
40° by 160°	$\delta\phi_p = 40°$	$\lvert\phi_p\rvert \in \{0°, 20°\},\ \theta_p \in \{80°\text{E, then every } 80° \text{ eastwards}\}$
	$\delta\theta_p = 160°$	$\lvert\phi_p\rvert \in \{10°, 30°\},\ \theta_p \in \{120°\text{E, then every } 80° \text{ eastwards}\}$
40° by 120°	$\delta\phi_p = 40°$	$\lvert\phi_p\rvert \in \{0°, 20°\},\ \theta_p \in \{90°\text{E, then every } 60° \text{ eastwards}\}$
	$\delta\theta_p = 120°$	$\lvert\phi_p\rvert \in \{10°, 30°\},\ \theta_p \in \{120°\text{E, then every } 60° \text{ eastwards}\}$
Zhou et al.	$\delta\phi_p = 20°$	$\lvert\phi_p\rvert \in \{0°, 20°\},\ \theta_p \in \{180°\text{W, then every } 40° \text{ eastwards}\}$
	$\delta\theta_p = 80°$	$\lvert\phi_p\rvert \in \{10°, 30°\},\ \theta_p \in \{160°\text{W, then every } 40° \text{ eastwards}\}$
Dong et al.	$\delta\phi_p = 30°$	$\lvert\phi_p\rvert \in \{0°, 15°, 30°\},\ \theta_p \in \{160°\text{W, then every } 40° \text{ eastwards}\}$
	$\delta\theta_p = 80°$	$\lvert\phi_p\rvert \in \{7.5°, 22.5°, 37.5°\},\ \theta_p \in \{180°\text{W, then every } 40° \text{ eastwards}\}$
Dong et al. shifted	$\delta\phi_p = 30°$	$\lvert\phi_p\rvert \in \{0°, 15°, 30°\},\ \theta_p \in \{180°\text{W, then every } 40° \text{ eastwards}\}$
	$\delta\theta_p = 80°$	$\lvert\phi_p\rvert \in \{7.5°, 22.5°, 37.5°\},\ \theta_p \in \{160°\text{W, then every } 40° \text{ eastwards}\}$
20° by 80°	$\delta\phi_p = 20°$	$\lvert\phi_p\rvert \in \{0°, 10°, 20°\},\ \theta_p \in \{140°\text{E, then every } 40° \text{ eastwards}\}$
	$\delta\theta_p = 80°$	$\lvert\phi_p\rvert \in \{5°, 15°, 25°\},\ \theta_p \in \{120°\text{E, then every } 40° \text{ eastwards}\}$